Manuel Martin-Pastor
C. Allen Bush
Department of Chemistry and Biochemistry, University of Maryland—Baltimore County, Baltimore, MD 21250

Received 13 January 2000; accepted 14 March 2000

Comparison of the Conformation and Dynamics of a Polysaccharide and of Its Isolated Heptasaccharide Repeating Unit on the Basis of Nuclear Overhauser Effect, Long-Range C–C and C–H Coupling Constants, and NMR Relaxation Data

Abstract: *A comparison of the conformation and dynamics of the cell wall polysaccharide of* S. mitis *J22 and the heptasaccharide repeating unit made from this polysaccharide was performed on the basis on nmr data. We have previously reported a model for this highly flexible polysaccharide in which four residues of the antigenic epitope adopt a defined conformation as do the two residues of the lectin-binding epitope. These domains are connected by a 6-substituted galactofuranoside residue that acts as a flexible hinge and the repeating subunits are joined by phosphodiester linkages that provide further flexibility. Homonuclear nuclear Overhauser effect (NOE) and long-range C–C and C–H scalar coupling constants measured in uniform* ^{13}*C-labeled samples of the polysaccharide and heptasaccharide were very similar, indicating a similar conformational average in solution. Significant differences in the solution dynamics were found from the heteronuclear relaxation data,* T_1, $T_{1\rho}$, *and NOE, which reflect the faster molecular tumbling of the heptasaccharide. Internal motions occurring on a picosecond time scale are relatively uniform along the polymer while dynamics on the time scale longer than a few nanoseconds is characteristic of hinge motion.* © 2000 John Wiley & Sons, Inc. Biopoly 54: 235–248, 2000

Keywords: *oligosaccharide; polysaccharide; conformation; dynamics; nmr spectroscopy*

INTRODUCTION

Bacterial cell surface polysaccharides, including capsules, cell wall polysaccharides, and lipopolysaccharide O-antigen chains, are typically synthesized with a subunit that repeats 20–100 or more times. The repeating unit can be as small as a single sugar residue (a homopolymer) but is often two or more residues. In most cases the subunits repeat regularly but in some bacterial strains, sugar residues are modified by O-acetylation or pyruvylation after their synthesis in a way which is not strictly stoichiometric perturbing the repeat.

The biological function of these polysaccharides often involves specific interactions of some carbohy-

Correspondence to: C. Allen Bush
Contract grant sponsor: National Science Foundation
Contract grant number: MCB9724133
Biopolymers, Vol. 54, 235–248 (2000)

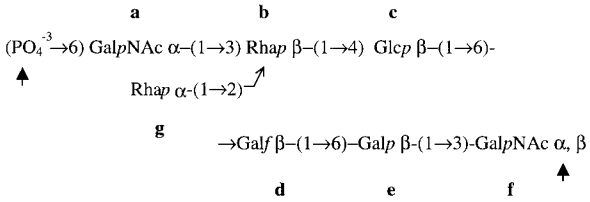

FIGURE 1 Structure of *S. mitis* J22 heptasaccharide repeating unit. Polymerization sites are indicated by black arrows.

drate epitope with a protein binding site. Examples of binding proteins might include a specific endoglycosidase produced by a bacteriophage, a specific lectin responsible for bacterial coaggregation, or binding of the bacteria to some host cell and antibodies whose interaction is important in pathogenesis. The relative sizes of the carbohydrates and the globular protein dictates a protein binding site of the order of two to four sugar residues, which is the approximate size of a carbohydrate binding epitope. This epitope may have a relatively fixed and well-defined three-dimensional conformation, as in the case of the blood group antigens, or the epitope could be flexible so that the protein binds to a conformation selected from among several preferred ones.[1] For polysaccharides whose repeating subunit is as large as six or eight sugar residues, there can be separate and distinct binding epitopes. The viridans streptococcal cell wall polysaccharides, with six to seven residues in the repeating unit, have two distinct epitopes with a lectin binding site [Gal $\beta(1 \rightarrow 3)$ GalNAc or GalNAc $\beta(1 \rightarrow 3)$ Gal] that is responsible for coaggregation with certain oral actinomyces species and a second epitope of three or four residues that binds antibodies.[2] These two epitopes are illustrated in Figure 1 for the cell wall polysaccharide of *Streptococcus mitis* J22 in which the antigenic epitope comprises residues **a, b, c**, and **g.**

The three-dimensional conformation of the biologically active epitope in a small isolated oligosaccharide need not be identical to that of the same sugar sequence in a higher molecular weight polysaccharide. Jennings and co-workers have demonstrated this feature, known as "conformational epitopes," using both immunological and physical techniques for both the meningococcal group B polysaccharide[3] and for the type III group B streptococcal polysaccharide.[4,5] We have previously presented evidence that such conformational epitopes are not found in the polysaccharide from *S. mitis* J22.[6] Nuclear Overhauser effect (NOE) patterns in the polysaccharide from J22 are similar to those in a heptasaccharide having a very similar structure.

While NOE data have been useful for studies of oligosaccharide conformation, a limited number of informative cross peaks is usually observed and there are ambiguities in the interpretation for flexible structures. Powerful new methods for conformational analysis involving ^{13}C enrichment of oligosaccharides and polysaccharides have been recently introduced that could provide a more complete and convincing picture of the conformation of complex oligosaccharides. Three-dimensional (3D) nmr methods having improved spectral resolution resulting from the greater dispersion in the ^{13}C dimension allow a better measure of NOE cross peaks. Moreover, ^{13}C coupling constants provide direct information on glycosidic dihedral angles giving explicit local conformation. With high ^{13}C enrichment it is possible to measure both C–H and C—C coupling constants providing several different scalar coupling values to report on the same dihedral angle to resolve ambiguities in correlation curves and provide statistical weights in cases of contributions of multiple conformations.[7]

Interpretation of long-range ^{13}C coupling constants requires a correlation curve relating the coupling constants to dihedral angles. Empirical correlations of the C–H coupling values[8] and of the C–C coupling values[9] have been proposed, and more recently, new quantum mechanical density function computational methods have been developed that greatly extend the usefulness and reliability of the scalar coupling correlation curves.[10–12]

The dynamics of complex polysaccharides are poorly understood with no clear model that can rationalize in structural terms the observations of widely varying nmr spectral line widths among different types of polysaccharides with different repeating subunit structures. The observation that certain 100 kD polysaccharides can give perfectly good nmr spectra with a few Hz line widths while others give line widths so broad as to be unobservable implies that the dynamics must depend strongly on details of the local stereochemistry. For proteins, dynamics have been investigated by heteronuclear relaxation rate studies of T_1, $T_{1\rho}$, and NOE with the results generally interpreted within the model-free analysis[13–15] in which the molecule is assigned an overall tumbling rate that is further modulated by internal motions on faster time scales. This model, which provides a reasonable picture for globular proteins, possibly might be applied to oligosaccharides of modest size, but it is less reasonable to apply it to a high molecular weight polysaccharide of extended or random global structure in which segmental motions could be present. For complex polysaccharides, certain segments of conserved local structure might rotate as a rigid entity

because of high amplitude torsional motions in other more flexible points along the repeating chain. For this case the relaxation data might better fit effective local correlation times for individual sugar residues instead of global correlation times when using the model free analysis. Other approaches to interpreting relaxation data for polysaccharides based on more explicit models for the internal motions of the polymer may be required to give a complete interpretation of the overall polymer dynamics.[16] In such a model the detailed stereochemistry of each sugar residue and linkage in the polymer is described by a reduced coordinate representation with a potential of mean force designed to simulate the linkage conformation and dynamics.[17]

In this paper, we report new scalar coupling and NOE data for the heptasaccharide from *S. mitis* J22, which can be readily compared with similar data on the intact polysaccharide. While the data show that the average conformations of the oligo- and polysaccharide are similar, heteronuclear relaxation data show significant differences in the dynamics. We also report new data for the intact polysaccharide, including some corrections to relaxation data previously reported by Xu et al.[18]

EXPERIMENTAL

Sample Preparation

Uniformly ~95% ^{13}C-enriched polysaccharide from S. *mitis* J22 (U-^{13}C J22 polysaccharide) and ~85% selective ^{13}C-enriched J22 polysaccharide at the anomeric positions (C-1–^{13}C J22 polysaccharide) were prepared by biosynthetic incorporation[19] and dissolved in D_2O at a concentration of 8 mg/mL corresponding to an approximate concentration of 8 m*M*.

A uniformly ^{13}C-labeled sample of the J22 heptasaccharide repeating unit (U–^{13}C J22 heptasaccharide; see Figure 1) was prepared by mild acid hydrolysis of the phosphodiester linkage attached at position C-1 of residue **f** in the polysaccharide,[20] using an ion exchange resin column (Dowex 50W-X2, Bio-Rad). Eight milligrams of the U–^{13}C J22 polysaccharide were dissolved in 0.5 mL and passed through this column using H_2O as eluent. Samples were collected from the column at regular intervals and the presence of the heptasaccharide was monitored by uv absorption at 200 nm. All the samples containing the heptasaccharide were combined together, lyophilized, exchanged three times in D_2O, and heated at 60°C for 4 h. Changes in the carbon decoupled ^{1}H-nmr spectrum showed the total disappearance of the signal of H-1**f** (5.482 ppm) in the polysaccharide and the appearance of a signal subsequently assigned as H-1$\mathbf{f}_\alpha$ (5.320 ppm) in the heptasaccharide. The U–^{13}C J22 heptasaccharide sample prepared (~8 mg in 0.5 mL of D_2O) was further characterized using other nmr experiments as the heptasaccharide of Figure 1 having a phosphate residue at C-6 for residue **a**. A natural abundance sample of J22 heptasaccharide in concentration ~ 17 mg/mL was prepared using the same protocol.

NMR Spectroscopy

Experiments were acquired at 500 MHz on a GE-Omega PSG 500 nmr instrument, or at 600 MHz in a GE-OMEGA 600 spectrometer. Data were processed on a Silicon Graphics workstation using Felix 2.3 software (MSI, San Diego, CA). All the cross peaks were assigned by matching chemical shifts of middle points and previously assigned spectra.[21]

Long-range ^{13}C–^{1}H scalar coupling data ($^nJ_{CH}$; $n > 1$) for U–^{13}C J22 polysaccharide were taken from previous work[18,19,22] (Table I). A t_1-coupled 3D-HMQC-NOESY (HMQC: heteronuclear multiple quantum correlation; NOESY: nuclear Overhauser effect spectroscopy) experiment[23] was acquired at 500 MHz for U–^{13}C J22 oligosaccharide at 15°C using a delay of 3.4 ms in the HMQC part to develop the heteronuclear antiphase magnetization and a NOE mixing time of 350 ms. The t_1-coupled 3D-HMQC-TOCSY[24] (TOCSY: total correlation spectroscopy) experiments were acquired for U–^{13}C J22 heptasaccharide at 25°C using a MLEV-17 mixing sequence with trim pulses[25] and a mixing time of 50 and 100 ms. For each 3D experiment the spectral width for both proton dimensions (t_2 and t_3) was 2500 Hz and for the carbon dimension (t_1) was 13158 Hz. A 3D matrix of 64 × 64 × 512 complex free induction decay (FID) points was acquired corresponding to $t_1 \times t_2 \times t_3$ dimensions. During data processing, each FID along both evolution dimensions (t_1 and t_2) was extended from 64 to 128 points with linear prediction before apodization by a 90° shifted sine-bell function. FIDs along t_1 were zero filled to 128 points, and those along t_2 and t_3 dimensions were zero filled to 1K data points. $^nJ_{CH}$ values for U-^{13}C J22 heptasaccharide were extracted from the relative displacement of the four E-COSY type cross peaks as described in previous work[19] and these data are given in Table I. One-bond $^1J_{CH}$ couplings for unlabeled J22 polysaccharide and heptasaccharide (Table II) were measured at 24°C from splittings in the indirect dimension of a t_1-coupled HSQC (heteronuclear single quantum coherence) experiment. In order to maximize the resolution in the indirect dimension, two sets of t_1-folded experiments were acquired, one with ^{13}C carrier position in the center of the anomeric region and the other in the center of the ring region (~75 ppm). Using this protocol the line width in the t_1 dimension at half height was ~12 Hz.

^{1}H–^{1}H NOEs were measured for U–^{13}C J22 polysaccharide and U-^{13}C J22 heptasaccharide samples by analyzing the two-dimensional (2D)-NOESY planes corresponding to different carbons atoms in the t_1-coupled 3D-HMQC-NOESY. The relative intensity of the diagonal peak with respect to each cross peak was qualified as s (strong), m (medium), or w (weak). ^{13}C—^{13}C long range coupling data

Table I Experimental Interresidue $^3J_{CH}$, $^3J_{CC}$, and $^2J_{CC}$ (Hz) for J22 Polysaccharide and Heptasaccharide

		ϕ			ψ		
Linkage		$^3J_{H1—C1—O1—Cx}$	$^3J_{C2—C1—O1—Cx}$	$^2J_{C1—O1—Cx}$ [b]	$^3J_{C1—O1—Cx—Hx}$	$^3J_{C1—O1—Cx—Cx-1}$	$^3J_{C1—O1—Cx—Cx+1}$
a—b	Hepta.	2.0	2.0	−1.7	1.7	<0.8	2.8
	Poly.[a]	1.5	1.7	−1.8	1.5	<0.8	2.5
b—c	Hepta.	0.9	2.5	−2.3	2.4	<0.8	2.2
	Poly.[a]	2.0	2.3	−1.8	2.1	<0.8	2.0
g—b	Hepta.	0.7	ol[c]	−2.3	4.3	ol	<0.8
	Poly.[a]	1.5	ol	−2.3	4.1	ol	<0.8
c—d	Hepta.	1.4	<0.8	−1.1	1.9	1.8	
	Poly.[a]	1.5	<0.8	−1.4	1.9	2.2	
d—e	Hepta.	1.5	2.1	−2.1	w[c]	2.6	
	Poly.[a]	1.5	2.6	−1.7	1.3	2.5	
e—f	Hepta.	w	ol	−2.5	w	lim[c]	<0.8
	Poly.[a]	2.4	ol	−2.0	1.3	lim	<0.8

[a] Literature values for J22 polysaccharide.[26,35]

[b] These values are assumed to be negative.

[c] ol: Overlapping signal; w: weak signal in 3D-HMQC-NOESY; lim: indicates that the ^{13}C chemical shift difference is too large for simultaneous excitation with our instrument.

Table II Experimental $^1J_{CH}$ (Hz) for J22 Polysaccharide and Heptasaccharide

Residue		H1—C1	H2—C2	H3—C3	H4—C4	H5—C5	H6—C6
a	Poly.	172.4	140.4	142.4	ol	145.2	150.2, 146.2
	Hepta.	173.4	141.3	143.3	148.1	146.0	144.0
b	Poly.	162.5	152.0	141.2	144.1	146.0	
	Hepta.	163.0	151.2	141.0	148.9	147.4	
g	Poly.	173.9	ol[c]	145.8	144.1	144.5	
	Hepta.	173.8	137.4	146.2	146.6	147.0	
c	Poly.	165.3	145.6	147.3	147.0	146.4	144.7, 144.3
	Hepta.	165.0	144.7	147.3	147.4	145.0	144.7
d	Poly.	175.5	149.6	149.6	148.1	147.5	155.4, 152.3
	Hepta.	174.5	149.8	149.2	150.8	146.4	150.3
e	Poly.	163.6	150.7	145.2	148.0	144.5	144.3, 142.7
	Hepta.	165.6	151.4	146.7	150.1	145.2	143.6
f	Poly.[a]	176.1	145.8	146.5	148.1	145.2	ol
	Hepta.[a]	171.0	139.9	147.1	149.8	143.7	ol
	Hepta.[b]	162.3	142.7	ol	149.0	144.7	ol

[a] Residue **f** anomer α.
[b] Residue **f** anomer β.
[c] ol: Overlapping signal.

($^nJ_{CC}$; $n > 1$) for U–^{13}C J22 polysaccharide were taken from previous work.[26] A similar pulse sequence[27] and experimental conditions were used to obtain the couplings of the anomeric signals for U–^{13}C J22 heptasaccharide at 600 MHz and 24°C. The refocusing delay T was set to 44 or 46 Hz to minimize the influence of $^1J_{CC}$ and the delay τ for transfer of magnetization by $^1J_{CH}$, was set to 168 Hz. Coupling constants between $C_{\mathbf{a}}$ and $C_{\mathbf{b}}$ were extracted, using Eq. (1), from the ratio of the cross-peak intensity $I_{\mathbf{Ha\text{-}Cb}}$ and direct peak $I_{\mathbf{Ha\text{-}Ca}}$.[27] Since this method does not offer information of the signs of the couplings, the sign was set to agree with the usual signs of these couplings in carbohydrates.

$$I_{\mathbf{Ha\text{-}Cb}}/I_{\mathbf{Ha\text{-}Ca}} = \tan^2(2\pi\, {}^nJ_{\mathbf{CaCb}}\, T) \qquad (1)$$

T_1, $T_{1\rho}$, and ^{1}H–^{13}C NOE relaxation data for C-1 ^{13}C J22 polysaccharide and natural abundance J22 heptasaccharide were acquired at 500 MHz and 24°C using the pulse sequences described by Kay et al.[28] The proton carrier frequency was set in the center of the proton spectrum with a spectral width of 2564.1 Hz. The ^{13}C carrier frequency was set in the middle of the anomeric region (~102 ppm) with a spectral width of 4000 Hz. Carbon decoupling during acquisition was carried out with WALTZ-16 with a field strength of 1612.9 Hz. Hard pulses were applied for proton and carbon with the INEPT delays corresponding to a nominal value of $^1J_{CH}$ of 165 Hz. The delays for T_1 relaxation varied between 10 and 400 ms, and those for the $T_{1\rho}$ measurement varied between 10 and 120 ms. NOE measurements were done by acquiring two spectra with and without proton presaturation during 2.5 s. For each relaxation experiment, a 2D matrix of 1024 × 64 complex FID data points was acquired for t_1 and t_2 dimensions.

Relaxation data for the uniformly enriched polysaccharide and heptasaccharide were obtained using the selective ^{13}C pulse scheme of Yamazaki et al.[29] as previously described.[18] The 2D FIDs were apodized in both dimensions with a 90° shifted sine-bell function and zero filled to give after Fourier transformation a 2D spectrum of 2048 × 128 real points. T_1 and $T_{1\rho}$ data were fitted using Origin software (Microcalc Origin v. 3.5, Microcalc Software, Inc.) to a two-parameter exponential function[28]:

$$I(t) = I_0 \exp^{-t/T} \qquad (2)$$

In this equation t is the delay time for relaxation, and T is either T_1 or $T_{1\rho}$.

The experimental T_1, $T_{1\rho}$, and ^{1}H–^{13}C NOE relaxation data of the unlabeled heptasaccharide and selectively labeled polysaccharide were analyzed in two different ways. In the first method, the relaxation data were fitted to several dynamical models according to the model free formalism[13–15] and several of its approximations, as described by Lommerse et al.[30] A complementary analysis of the relaxation data was done using the reduced spectral density function method.[31–33] The application of the latter method to ^{1}H–^{13}C relaxation data has been previously described.[18] In both analyses it was assumed that relaxation is exclusively dipolar.

A simplex method was used to fit the experimental T_1, $T_{1\rho}$ and ^{1}H–^{13}C NOE to several dynamical models including the original model-free formalism proposed by Lipari and Szabo[13–15]and several approximations as described by Lommerse et al.[30]—all of which assume that relaxation is exclusively dipolar. Model I is rigid isotropic motion with a global correlation time τ_o. Model II has a two-parameter fit with a global correlation time τ_o and an order parameter S^2

to describe the flexibility of fast internal motions in each residue. In model III, different residues of the carbohydrate may tumble independently with a different effective correlation time assigned to each residue (τ_{eff}). Model IV was fit using different effective correlation time (τ_{eff}) and order parameter S^2 for each residue. Model V is the regular model-free approach described by Lipari and Szabo[13] with a global correlation time τ_o and two parameters S^2 and τ_{int} for internal motions.

For each dynamical model, the following error function R_ω was used to evaluate the quality of the fit:

$$R_\omega = \sqrt{\sum_{i=1}^{n} \frac{k_1(T_1^{calc} - T_1^{exp})^2 + k_2(T_{1\rho}^{calc} - T_{1\rho}^{exp})^2 + k_3(NOE^{calc} - NOE^{exp})^2}{(T_1^{exp})^2 + (T_{1\rho}^{exp})^2 + (NOE^{exp})^2}} \quad (3)$$

In Eq. (3), the summation extends over n residues; k_1, k_2 and k_3 are coefficients used to weight the experimental error in the data.[34] The data were minimized with $k_1 = 1$, $k_2 = 1$, and $k_3 = 1$. A set of 10,000 Monte Carlo generated starting parameters was used to avoid being trapped in false minima during this nonlinear optimization. An estimation of the uncertainties in the motional parameters was performed from these results. These calculations were performed with in-house software available upon request.

RESULTS AND DISCUSSION

The U–^{13}C J22 heptasaccharide was obtained by mild acid hydrolysis of the glycosidic phosphate linkage connecting the repeating units of the U–^{13}C polysaccharide (Figure 1). Chemical shifts were very similar to those in the polysaccharide with differences from the values reported for the J22 polysaccharide[21] $\leq \pm 0.1$ ppm and ± 0.5 ppm for proton and carbons, respectively. The most notable difference in the oligomer is the appearance of a new set of signals in residue **f** (GalNAc) corresponding to reducing terminal α and β anomers ($\sim$ 80:20), which were assigned based on the corresponding $^1J_{C1\text{-}H1}$ values (Table II), and a difference of $+2.8$ ppm in the carbon chemical shift of C-1$\mathbf{f}_\alpha$ (92.4 ppm) with respect to the same signal in the polysaccharide.[21] Since chemical shifts are extremely sensitive to conformation and no other major differences in chemical shifts were found, these results suggest that no major conformational changes should be expected between the J22 heptasaccharide and polysaccharide.

Further information regarding conformation is provided by interring ^{1}H–^{13}C long range ($^nJ_{CH}$; $n > 1$) and ^{13}C–^{13}C long-range ($^nJ_{CC}$; $n > 1$) coupling constants, which are related to the torsion angles ϕ and ψ of the glycosidic linkages. $^nJ_{CH}$ couplings were measured in t_1-coupled 3D-HMQC-NOESY and 3D-HMQC-TOCSY experiments for the U–^{13}C J22 heptasaccharide and were compared with $^nJ_{CH}$ data for the U–^{13}C J22 polysaccharide previously reported[19,22] (Figure 2, Table I). $^nJ_{CC}$ were measured[27] for the anomeric peaks of the J22 oligosaccharide and were compared with values previously reported for the J22 polysaccharide[26] (Figure 3, Table I). It can be seen in Table I that the interglycosidic $^nJ_{CH}$ couplings for the heptasaccharide and polysaccharide are very similar, in most cases within the experimental error, which is estimated to be ± 0.5 Hz. The only two exceptions are the $^3J_{H1\text{-}C1\text{-}O1\text{-}Cx}$ between residues **b—c** for which the difference is 1.1 Hz and $^3J_{H1\text{-}C1\text{-}O1\text{-}Cx}$ between residues **g—b** for which the difference is 0.8 Hz. Although these differences could be related to a small change in the conformation of torsions $\phi_{\mathbf{bc}}$ and $\phi_{\mathbf{gb}}$, this interpretation is not supported by the $^nJ_{CC}$ coupling data in Table I, which does not differ significantly. In all cases the differences observed for the interring $^nJ_{CC}$ data (Table I) of the J22 polysaccharide and heptasaccharide are relatively small ($\leq$0.6 Hz). Previous conformational studies of the J22 polysaccharide based on these same nmr experimental data and molecular mechanics calculations[7,35] found a flexible model with three major conformers in solution. The principal differences among the three conformers were in the glycosidic angles $\phi_{\mathbf{bc}}$, $\phi_{\mathbf{cd}}$, $\psi_{\mathbf{cd}}$, and $\phi_{\mathbf{de}}$, $\psi_{\mathbf{de}}$ with similar values for the other glycosidic torsion angles. The similarities found between the interring coupling data of the J22 heptasaccharide and polysaccharide indicate that a similar flexible model would also be consistent with the data for the heptasaccharide.

Conformational information for the intraresidue ring puckering of the pyranose and furanose rings in the J22 polysaccharide can be obtained from the one-bond $^1J_{CH}$ measured in t_1-coupled HSQC experiments (Table II), the intraring $^nJ_{CC}$ obtained in the quantitative coherence transfer method[27] (Table III), and the intraresidue $^nJ_{CH}$ from the t_1-coupled 3D-HMQC-NOESY and 3D-HMQC-TOCSY experiments (data not show). A comparison of the $^1J_{CH}$ values in Table II reveals that differences between the J22 polysaccharide and oligosaccharide are $\leq$1.0 Hz in most cases. The only exception occurs for the values of $^1J_{H1\text{-}C1f\alpha}$ and $^1J_{H2\text{-}C2f\alpha}$ in the heptasaccharide which differ by -5.1 and 5.9 Hz from the polysaccharide, differences that can be explained by the lack of the phosphate group attached to C-1 in the J22 heptasaccharide. No consistent variation in the $^1J_{CH}$ couplings were found that could indicate that there is a change in the ring puckering. The intraring $^nJ_{CC}$ couplings (Table III) which are very similar in the J22 polysac-

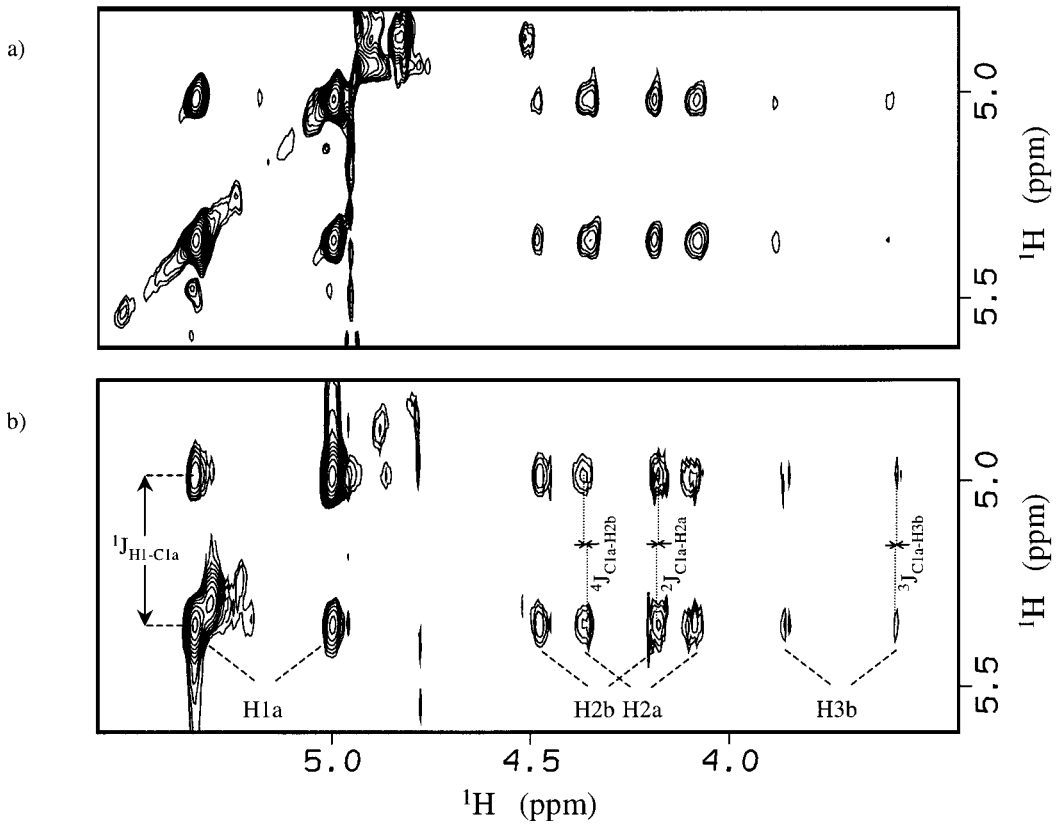

FIGURE 2 NOESY plane corresponding to C-1a carbon taken from t_1-coupled 3D-HMQC-NOESY experiments used to measure the long-range $^nJ_{CH}$ scalar couplings in (a) the U–^{13}C J22 heptasaccharide and (b) the U–^{13}C J22 polysaccharide.

charide and heptasaccharide confirm this conclusion, and are consistent with values found in the literature for similar monosaccharide rings. Long-range intraresidue $^nJ_{CH}$ values were also very similar (data not shown). Previous nmr studies based on the intraring $^nJ_{CH}$, $^nJ_{CC}$, ^{1}H–^{1}H NOE, and the vicinal intraresidual $^3J_{HH}$[7, 35] showed that these experimental data are consistent with normal $^1C_4$ or $^4C_1$ chair conformations for the pyranose sugar rings of the J22 polysaccharide while the Gal*f* furanose ring **d** has been found to exclusively adopt conformations ^{1}E or $^1T_2$ of the pseudorotational cycle.[7]

^{1}H–^{1}H interglycosidic NOEs for J22 polysaccharide and heptasaccharide were measured qualitatively from the t_1-coupled 3D-HMQC-NOESY (Figure 2) and the results are given in Table IV. Normalized ^{1}H–^{1}H NOE intensities measured previously[36] for the U–^{13}C J22 polysaccharide using a decoupled 3D-HMQC-NOESY experiment with a similar mixing time and temperature, and were included in Table IV for comparison. Despite possible differences in dynamics of the polymer and oligomer, it can be seen in Table IV that similar interglycosidic NOE were obtained, suggesting a similar conformation for the polysaccharide and heptasaccharide in solution.

The T_1 and $T_{1\rho}$ relaxation parameters obtained from the exponential fit of the relaxation experiments (see Figure 4) and ^{1}H–^{13}C NOE for the different samples of J22 polysaccharide and heptasaccharide are given in Table V.We have previously reported relaxation data for the U–^{13}C J22 polysaccharide. [18] While the $T_{1\rho}$ relaxation data obtained here for the polysaccharide (Table V) were similar to those previously reported for the U–^{13}C J22 polysaccharide,[18] the T_1 data differ due to an error in the analysis of the data in the earlier report. The NOE values reported here are consistently larger apparently due to a problem of truncated saturation in the earlier ^{1}H–^{13}C NOE experiments as a result of the reduced power level used during the application of selective soft pulses during the saturation which resulted in a reduction of the magnitude of NOE.[29] Table V also includes relaxation data for a selectively C-1 ^{13}C-enriched sample of J22 polysaccharide as a control for artifacts in the uniformly enriched sample resulting from cross relaxation effects and C_1—C_2 autocorrelation. The

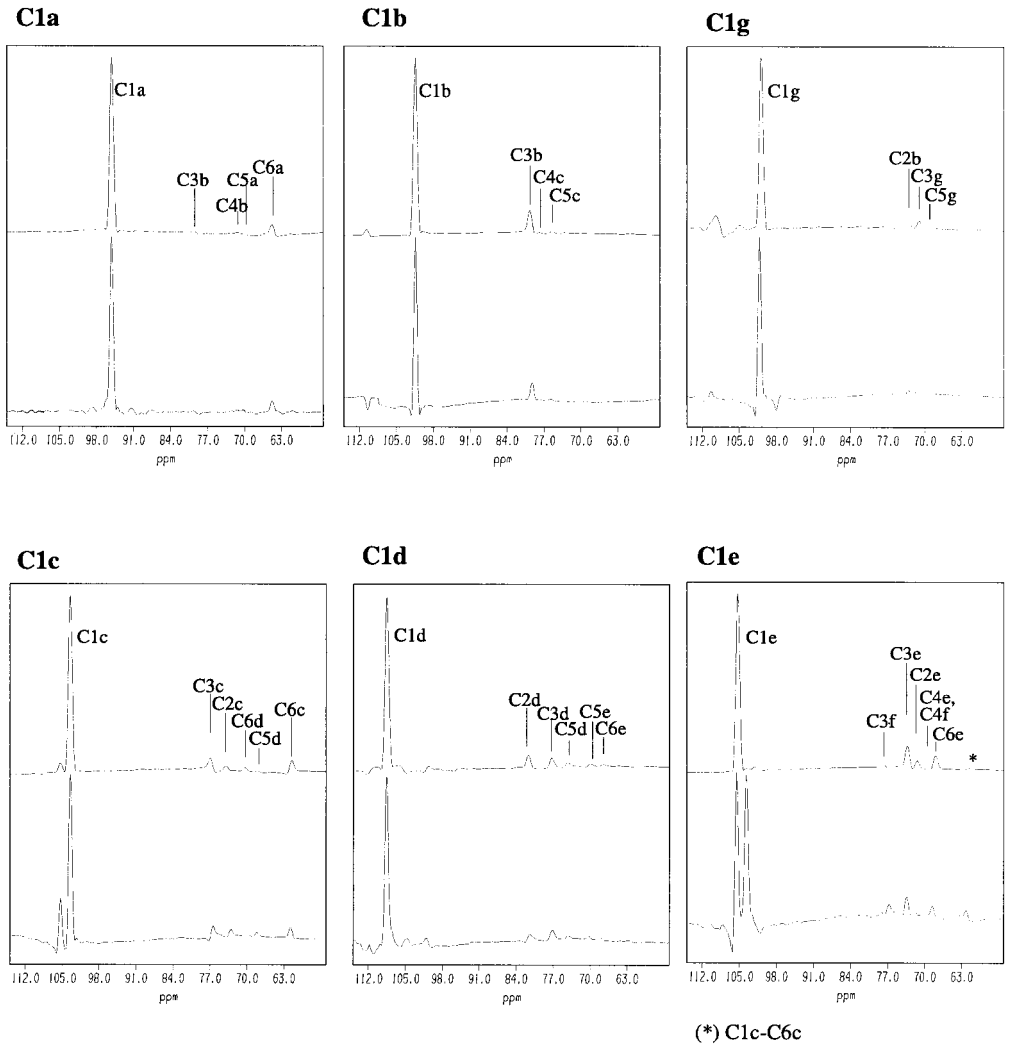

FIGURE 3 One-dimensional slices for the different anomeric signals of J22 taken from the 2D quantitative $^{n}J_{CC}$ experiments (upper slice) U–^{13}C J22 polysaccharide and (lower slice) U–^{13}C J22 heptasaccharide.

agreement between the two sets of data argues that the selective ^{13}C pulse scheme used is effective in avoiding these artifacts.[18,29] Table V includes two sets of relaxation data for the heptasaccharide, one for a uniformly highly enriched sample measured using the selective pulse scheme of Yamazaki et al.[29] and one for a natural abundance sample using conventional inverse detection pulse sequence.[28] Although cross-correlation could possibly interfere with the relaxation data for the uniformly ^{13}C-enriched heptasaccharide, it is at a lower concentration than the natural abundance sample so is less subject to effects of viscosity. The good agreement between the two sets of data argues that neither of these effects interfere significantly with the measurements.

Inspection of the data of Table V reveals that the T_1 values for the different residues of the polysaccharide are rather similar. Although T_1 values for residues **c** and **d** are slightly longer than for the other residues, $T_{1\rho}$ for residue **d** is significantly longer than for the other residues. For the heptasaccharide the differences in T_1 and $T_{1\rho}$ among the residues is smaller and not significantly outside the estimated experimental error. Comparison of the T_1 and $T_{1\rho}$ for the heptasaccharide and polysaccharide shows they are similar while the NOE for the heptasaccharide are generally significantly larger than those for the polysaccharide.

The subtle differences in the relaxation data are reflected in the reduced spectral density analysis which follows Farrow et al.[31–33] This method assumes that the high-frequency spectral density terms are of approximately equal magnitude, i.e., $J(\omega_H \pm \omega_C) \sim J(\omega_H)$, so that it is possible from measurements of three relaxation rates to determine the value of the

Table III Intraresidue $^nJ_{cc}$ (Hz) for U–^{13}C J22 Heptasaccharide and U–^{13}C J22 Polysaccharide

Atom Pair	Hepta.	Poly.[a]	Lit.[b]	Atom Pair	Hepta.	Poly.[a]	Lit.[b]
C-1**a**—C-3**a**	0	0	0	C-1**c**—C-5**c**	0	0	0
C-1**a**—C-4**a**	0	0	0	C-1**c**—C-6**c**	3.43	3.68	4.1
C-1**a**—C-5**a**	1.39	1.64	1.9	C-1**d**—C-3**d**	3.02	3.42	—
C-1**a**—C-6**a**	3.64	3.48	3.6	C-1**d**—C-4**d**	0	0	—
C-1**b**—C-3**b**	4.23	5.05	4.0	C-1**d**—C-5**d**	1.42	1.79	—
C-1**b**—C-4**b**	0	0	0	C-1**e**—C-3**e**	5.03	4.9	4.6
C-1**b**—C-5**b**	0	0	0	C-1**e**—C-4**e**	0	0	0
C-1**b**—C-6**b**	lim[c]	lim[c]		C-1**e**—C-5**e**	0	0	0
C-1**g**—C-3**g**	0.42	0	0	C-1**e**—C-6**e**	4.72	4.20	4.4
C-1**g**—C-4**g**	0	0	0	C-1$\mathbf{f}_\alpha$—C-3$\mathbf{f}_\alpha$	0	0	0
C-1**g**—C-5**g**	1.25	1.53	2.0	C-1$\mathbf{f}_\alpha$—C-4$\mathbf{f}_\alpha$	0	0	0
C-1**g**—C-6**g**	lim[c]	lim[c]		C-1$\mathbf{f}_\alpha$—C-5$\mathbf{f}_\alpha$	1.97	1.98	1.9
C-1**c**—C-3**c**	4.41	4.25	4.5	C-1$\mathbf{f}_\alpha$—C-6$\mathbf{f}_\alpha$	3.95	3.57	3.6
C-1**c**—C-4**c**	0	0	0				

[a] Literature values for J22 polysaccharide.[26]
[b] Literature values from data on similar sugars.[43]
[c] lim: ^{13}C chemical shift difference is too large for simultaneous excitation with our instrument.

spectral density function at three frequencies $J(0)$, $J(\omega_C)$, and $J(\omega_H)$.[31] The errors indicated in Table VI and Figure 5 were estimated by a Monte Carlo method in which random variations up to the experimental error were applied. For the polysaccharide $J(0)$ for residue **d** is lower than for the other residues while $J(\omega_C)$ remains high. We interpret this result as an indication of greater mobility on the nanosecond time scale for residue **d** when compared to other residues in the polymer. A similar conclusion was drawn from our earlier studies on the polysaccharide.[18]

Table IV Interglycosidic Qualitative Strong (s) and Medium (m) ^{1}H–^{1}H NOEs Measured for U–^{13}C J22 Polysaccharide and U–^{13}C Heptasaccharide

Proton Pair	Lit. Poly.[a]	Poly.	Hepta.
H1**a**—H1**g**	0.0130	m	m
H1**a**—H2**b**	0.0340	s	s
H1**a**—H3**b**	0.0159	m	m
H5**a**—H3**b**	0.0256	m	m
H1**b**—H3**c**	0.0197	m	m
H1**b**—H4**c**	0.0437	s	s
H1**g**—H2**b**	0.0231	m	m
H1**c**—H6$\mathbf{d}_{\text{pro-R}}$	0.0226	m	m
H1**c**—H6$\mathbf{d}_{\text{pro-S}}$	0.0313	s	s
H1**d**—H6$\mathbf{e}_{\text{pro-R}}$	0.0129	m	m
H1**d**—H6$\mathbf{e}_{\text{pro-S}}$	0.0099	m	m
H1**e**—H3$\mathbf{f}_\alpha$	0.0282	s	s

[a] Normalized ^{1}H–^{1}H NOE values for J22 polysaccharide taken from Ref. 35.

For the heptasaccharide, $J(0)$ values are more uniform among the seven residues. Most studies of oligosaccharides have concluded that there is greater mobility for the end residues compared to the interior ones. It appears that these end effects contribution to mobility approximately equals the greater mobility of the central residue **d** leading to similar spectral density parameters for all the residues of the heptasaccharide.

Figure 6 shows simulated relaxation data at 500 MHz as a function of the global correlation time (τ_o) of the molecule for the model-free approach.[13] If segmental motions are present in the oligo- and/or polysaccharide, τ_o would represent the effective correlation time τ_{eff} of a single sugar residue.[30] Two cases are illustrated, one corresponding to a very flexible molecule/residue with fast internal motions ($S^2 = 0.6$, $\tau_{int} = 100$ ps) and the other to the case of a rigidly tumbling molecule/residue ($S^2 = 1.0$). The T_1 values in Table V are near the minimum value and do not rise above 0.35 s, implying that τ_o is less than 5 ns. Table V shows that the ^{1}H–^{13}C NOE data for the heptasaccharide are generally larger than for the polysaccharide. This must result from faster overall tumbling (or effective correlation times) for the oligosaccharide with τ_o in the 0.5–2 ns range. It can be seen in Figure 6 that the contribution of the fast internal motion (on the ps time scale) tends to decrease the ^{1}H–^{13}C NOE since it is too rapid to be effective in causing relaxation responsible for NOE.

The relaxation data were also interpreted by fitting to several dynamical models which are variants of the

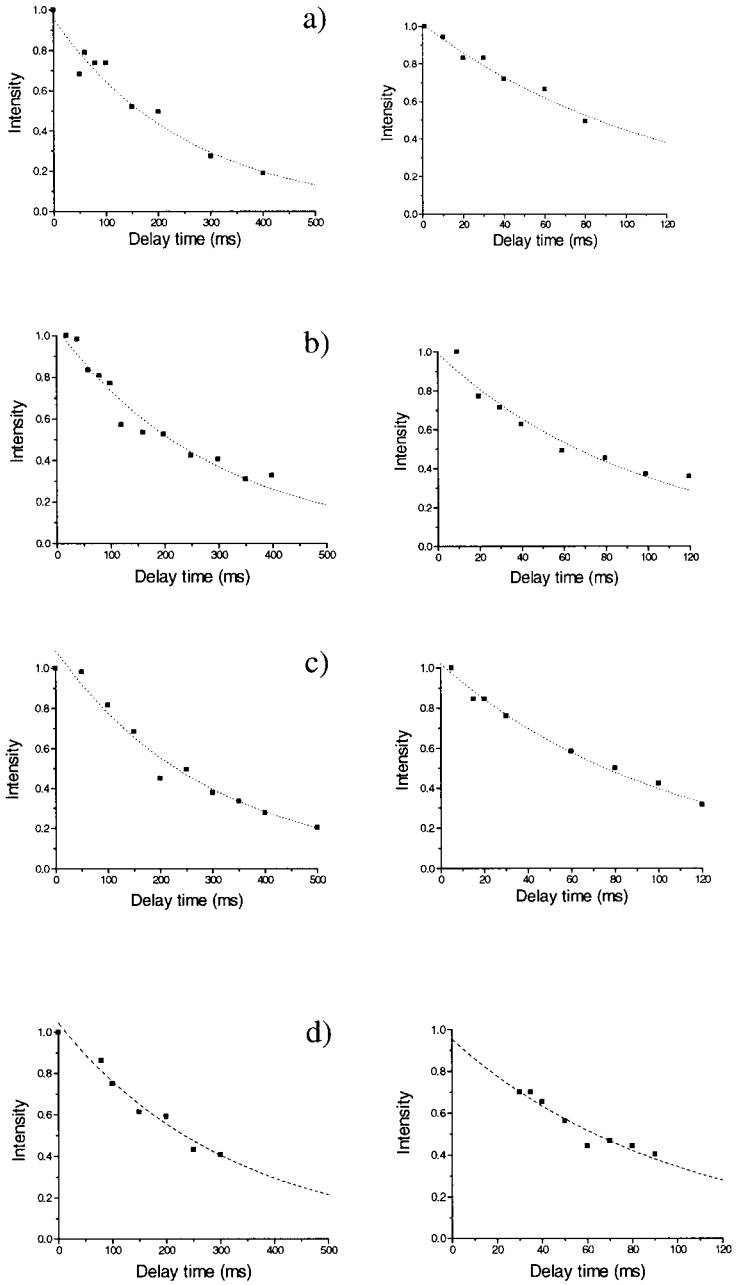

FIGURE 4 $^{1}H–^{13}C$ T_1 and $T_{1\rho}$ relaxation decay curves as a function of the delay time (ms) for the anomeric carbon of residue **d** in (a) the U–^{13}C J22 heptasaccharide, (b) the U–^{3}C J22 polysaccharide, (c) the C-1–^{13}C J22 polysaccharide, and (d) the unlabeled J22 heptasaccharide.

"model-free" formalism[13–15] by using the spectral density functions described by Lommerse et al.[30] The results given in Table VII show that, independent of the model chosen, the correlation times obtained for the polysaccharide are larger than those in the heptasaccharide, in agreement with the qualitative analysis based on Figure 6. Larger values of the error parameter R_ω are found when the data are fitted using the most rigid models I and II compared to the more flexible models III–V for which the difference in R_ω is not statistically relevant. Values of τ_{eff} obtained in the fit using models III and IV are in the range ~500–1500 ps for the polysaccharide and 300–550 ps in the heptasaccharide.

While the tumbling times in Table VII agree with the more qualitative analysis above, the order parameters for fast internal motion (S^2) depend on the dynamic model considered. These results suggest, in

Table V $^{1}H–^{13}C$ T_1 (s), $T_{1\rho}$ (s) and NOE Relaxation Experimental Data Obtained for the Different Anomeric Signals of U–^{13}C J22 Heptasaccharide and Polysaccharide, and Unlabeled J22 Heptasaccharide and C-1–^{13}C J22 Polysaccharide

	U–^{13}C Hepta.			U–^{13}C Poly.		
Residue	T_1[a]	$T_{1\rho}$[a]	NOE[b]	T_1[a]	$T_{1\rho}$[a]	NOE[b]
C-1**a**	0.30	0.11	1.64	0.28	0.10	1.35
C-1**b**	0.26	0.12	1.71	0.25	0.09	1.66
C-1**g**	0.30	0.12	1.78	0.25	0.09	1.66
C-1**c**	0.35	0.13	2.01	0.33	0.12	1.21
C-1**d**	0.25	0.12	2.02	0.33	0.19	1.54
C-1**e**	0.32	0.13	1.91	0.29	0.14	1.23
C-1$\mathbf{f}_\alpha$	0.30	0.13	2.25	0.31	0.11	1.58
	Unlabeled Hepta.			C-1–^{13}C Poly.		
Residue	T_1	$T_{1\rho}$	NOE[b]	T_1[b]	$T_{1\rho}$[b]	NOE[b]
C-1**a**	0.31[a]	0.10[a]	1.83	0.30	0.11	1.42
C-1**b**	0.25[b]	0.11[b]	2.06	0.24	0.09	1.76
C-1**g**	0.32[c]	0.12[b]	1.67	0.24	0.08	1.54
C-1**c**	0.33[b]	0.12[c]	1.71	0.34	0.13	1.28
C-1**d**	0.29[a]	0.10[b]	2.07	0.34	0.17	1.54
C-1**e**	0.30[b]	0.13[b]	2.14	0.29	0.13	1.25
C-1$\mathbf{f}_\alpha$	0.31[a]	0.13[a]	2.03	0.29	0.09	1.42

[a] Exp. error ± 0.03.
[b] Exp. error ± 0.01.
[c] Exp. error ± 0.02.

agreement with the qualitative analysis of the relaxation data, that variations in fast internal motion (less than 100 ps time scale) do not explain the trends in the relaxation data and that motions on a time scale longer than 1 ns are the origin of the differences.

CONCLUSIONS

We have previously reported $^{1}H–^{1}H$ NOE data on a heptasaccharide from *S. gordoni* 38 whose structure differs from that of the J22 oligosaccharide (Figure 1) only in that the sequence of the two residues (Gal and GalNAc) at the reducing terminal is reversed.[6] The present results, which include ^{13}C coupling data, confirm and extend the conclusions from that paper that the polysaccharide from *S. mitis* J22 does not have a conformational epitope. Immunological data also support the conclusion that the epitopes have similar conformations in the oligosaccharide and polysaccharide.[2]

Table VI Reduced Spectral Density Terms $J(0)$, $J(\omega_C)$, and $J(\omega_H)$ (in ns · rad^{-1}) Calculated from the Relaxation Data of the Different Anomeric Signals of Unlabeled J22 Heptasaccharide and C-1 ^{13}C-labeled J22 Polysaccharide

	Unlabeled Hepta.			C-1–^{13}C Poly		
Residue	$J(0)$	$J(\omega_C)$	$J(\omega_H)$	$J(0)$	$J(\omega_C)$	$J(\omega_H)$
C-1**a**	7.3 ± 1.4	3.6 ± 0.1	0.63 ± 0.03	6.5 ± 1.2	4.5 ± 0.2	0.33 ± 0.02
C-1**b**	4.1 ± 1.1	3.9 ± 0.2	0.99 ± 0.05	6.4 ± 1.5	4.7 ± 0.2	0.73 ± 0.04
C-1**g**	5.4 ± 1.0	3.7 ± 0.1	0.48 ± 0.02	8.4 ± 1.9	5.2 ± 0.2	0.52 ± 0.03
C-1**c**	5.4 ± 0.9	3.6 ± 0.1	0.5 ± 0.02	5.4 ± 0.8	4.0 ± 0.1	0.19 ± 0.01
C-1**d**	5.7 ± 1.3	3.4 ± 0.1	0.88 ± 0.04	2.7 ± 1.0	3.6 ± 0.2	0.36 ± 0.03
C-1**e**	4.0 ± 0.9	3.1 ± 0.1	0.89 ± 0.04	4.4 ± 1.6	4.9 ± 0.4	0.20 ± 0.03
C-1$\mathbf{f}_\alpha$	4.2 ± 0.9	3.2 ± 0.1	0.78 ± 0.03	8.0 ± 1.5	4.5 ± 0.2	0.33 ± 0.01

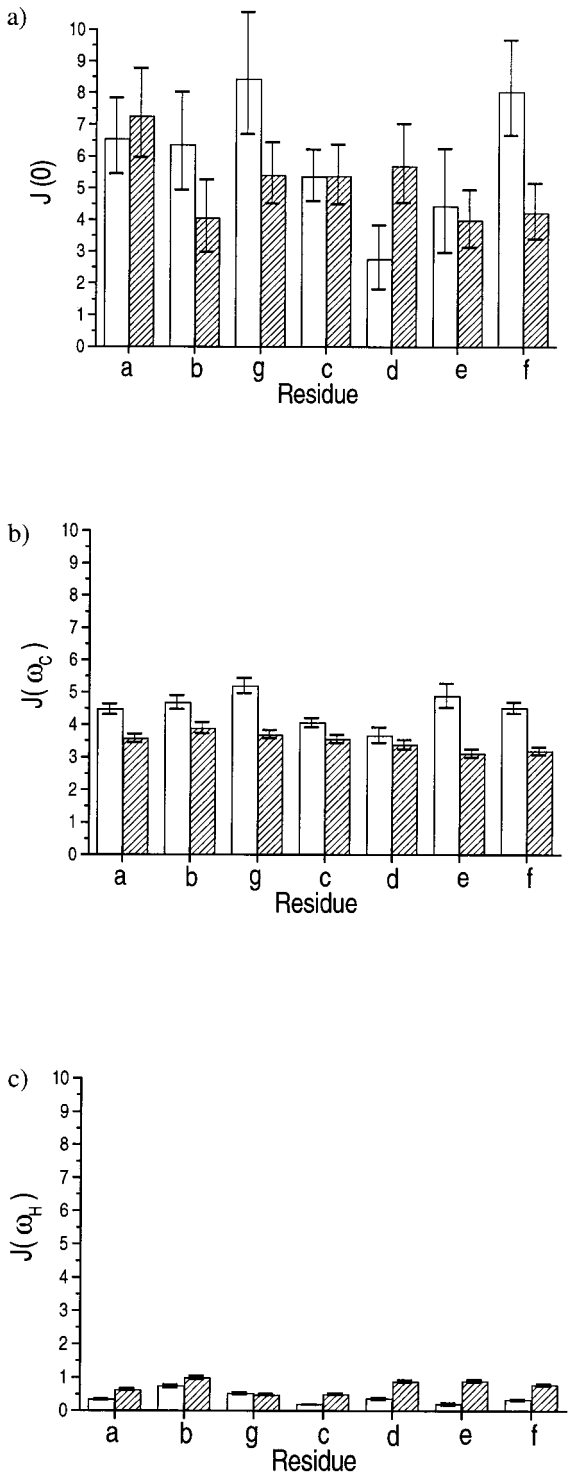

FIGURE 5 Plots of the spectral density terms (a) $J(0)$, (b) $J(\omega_C)$, and (c) $J(\omega_H)$ (in ns · rad^{-1}) calculated for the anomeric ^{13}C signals of the different residues of J22. J22 polysaccharide (white bars) and J22 heptasaccharide (stripped bars). Errors bars are also included.

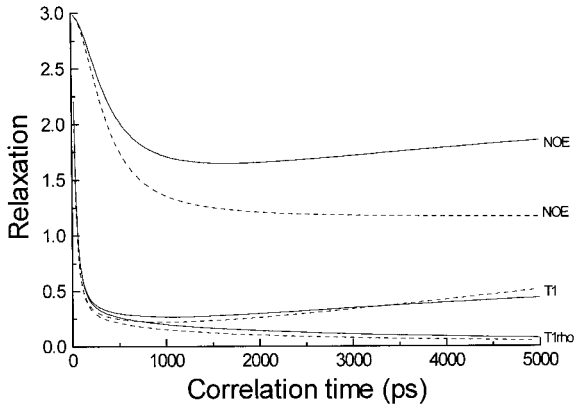

FIGURE 6 Theoretical curves at 500 MHz for ^1H–^3C T_1, $T_{1\rho}$, and NOE as a function of global correlation time for a rigid molecule ($S^2 = 1$; continuous line) and a flexible molecule ($S^2 = 0.6$, $\tau_{int} = 100$ ps) in the model-free approach[13] (segmented line).

Our ^{13}C relaxation data on the C-1 ^{13}C-enriched polysaccharide confirms the validity of the use of selective ^{13}C pulses for measuring relaxation data on uniformly enriched carbohydrates.[18,29] In spite of an unfortunate error in the earlier ^{13}C relaxation data, the qualitative conclusions of that work are confirmed. Analysis of the corrected data reported here argues that there is increased motion on the ns time scale for the galactofuranoside residue **d** in the *S. mitis* J22 polysaccharide. Recent molecular modeling results show that this increased flexibility does not arise from puckering motions of the furanoside ring, which adopts a preferred conformation in the ^1E or $^1T_2$ region.[7] The observed motions on the ns time scale could be about the glycosidic linkages and the C4—C5 and C5—C6 bonds in the 1–6 substituted furanoside.

While polysaccharides must have internal motion, it is the nature of that motion and its time scale that remain unclear. The fast internal motion revealed in solvated molecular dynamics simulations is in good agreement with nmr data.[36–39] But such motion in the ps range is exhibited to a similar extent by all pyranosides and does not vary much from residue to residue. The motions responsible for variations in the nmr line widths among different carbohydrate structures must arise from differences in segmental motion involving several sugar residues. Our observation that τ_{eff} for the polysaccharide is only slightly larger than that for the heptasaccharide argues that these segments must be of the order of 3–10 residues, a value consistent with estimates of persistence lengths for some other polysaccharides.[40] While these conclusions might not be universally applicable to all polysaccharides, the relaxation data reported here for the

Table VII Best Fit of the $^{1}H–^{13}C$ Relaxation Data for Dynamic Models I–V for the Different Anomeric Signals of C-1–^{13}C J22 Polysaccharide and Unlabeled J22 Heptasaccharide

	C-1–^{13}C Poly.					Unlabeled Hepta.				
Model	I[a]	II[b]	III[c]	IV[d]	V[e]	I[a]	II[b]	III[c]	IV[d]	V[e]
R_ω	0.126	0.122	0.048	0.047	0.031	0.109	0.109	0.064	0.064	0.078
τ_0 (ns)	0.8	0.8			2.8	0.41	0.41			0.51
Residue	S^2	τ_{eff} (ps)		τ_{eff} (ps)	S^2	S^2	τ_{eff} (ps)		τ_{eff} (ps)	S^2
C-1**a**	0.93	875		875	0.79	1.0	467		467	0.91
C-1**b**	1.00	510		510	0.60	1.0	364		364	0.60
C-1**g**	1.00	699		699	0.69	1.0	566		568	1.00
C-1**c**	0.79	1310		1341	0.75	1.0	537		539	1.00
C-1**d**	0.74	684		685	0.61	1.0	359		359	0.60
C-1**e**	0.90	1478		1518	0.88	1.0	333		333	0.60
C-1$\mathbf{f}_\alpha$	0.97	880		879	0.79	1.0	373		372	0.62

[a] $\tau_0 \pm 0.01$ ns.
[b] $\tau_0 \pm 0.01$ ns, $S^2 \pm 0.02$.
[c] $\tau_{eff} \pm 10$ ps.
[d] $\tau_{eff} \pm 10$ ps, $S^2 > 0.87$ for all residues.
[e] $\tau_0 \pm 0.02$ ns, $S^2 \pm 0.03$, $\tau_{int} < 150$ ps for all residues.

J22 heptasaccharide does not differ greatly from those reported for some other complex oligosaccharides.[38,41,42]

Unfortunately, our results tell us only that these important motions in polysaccharides must be on a time scale of at least a few ns and they could be as slow as 100s of ns. In either case, these motions do not lend themselves to treatment by the model-free approach of Lipari and Szabo.[13] While this method has been widely used for analysis of nmr relaxation data on both oligosaccharides and polysaccharides, it is difficult to distinguish between effects of anisotropy and internal motion in this model and coupling among internal motions in polysaccharides seriously compromises the basic assumptions of the treatment. The reduced spectral density analysis fails to give any detailed molecular interpretation of the data. It is most likely that a more complex model for the motions, such as that described by Perico et al.[17] will be needed to relate dynamics to detailed linkage stereochemistry of carbohydrates. Unfortunately, application of this theory to a complex heteropolysaccharide poses a daunting challenge.

This research was supported by National Science Foundation Grant MCB9724133 and by a postdoctoral fellowship from Ministerio de Educacion y Cultura of Spain to MMP.

We thank Dr. M. F. Summers for providing the observation time on the GE-Omega 600 spectrometer and Ms. Charlene Ton for preparing the C-1 ^{13}C-labeled sample of the J22 polysaccharide. We thank Dr. J. O. Cisar for providing the natural abundance sample of J22 of polysaccharide and for continued advice and encouragement on this project.

REFERENCES

1. Bush, C. A.; Martin-Pastor, M.; Imberty, A. Annu Rev Biophys Biomol Struct 1999, 28, 269–293.
2. Cisar, J. O.; Sandberg, A. L.; Reddy, G. P.; Abeygunawardana, C.; Bush, C. A.; Infect Immun 1997, 65, 5035–5041.
3. Evans, S. V.; Sigurskjold, B. W.; Jennings, H. J.; Brisson, J. R.; To, R.; Tse, W. C.; Altman, E.; Frosch, M.; Weisbgerber, C.; Kratzin, H. D.; Klebert, S.; Vaesen, M.; BitterSuermann, D.; Rose, D. R.; Young, N. M.; Bundle, D. R. Biochemistry, 1995, 34, 6737–6744.
4. Brisson, J.-R.; Uhrinova, S.; Woods, R. J.; Zwan, M.; Jarrel, H. C.; Paoletti, L. C.; Kasper, D. L.; Jennings, H. J. Biochemistry, 1997, 36, 3278–3292.
5. Zou, W.; Mackenzie, R.; Therien, L.; Hirama, T.; Yang, Q.; Gidney, M. A.; Jennings, H. J. J Immunol 1999, 163, 820–825.
6. Xu, Q. W.; Gitti, R.; Bush, C. A. Glycobiology, 1996, 6, 281–288.
7. Martin-Pastor, M.; Bush, C. A. Biochemistry, 1999, 38, 8045–8055.
8. Tvaroska, I.; Hricovini, H.; Perakova, E. Carbohydr Res 1989, 189, 359–362.
9. Milton, M. J.; Harris, M. A.; Probert, M. A.; Field, R. A.; Homans, S. W. Glycobiology, 1998, 8, 147–153.
10. Bose, B.; Zhao, S.; Stenutz, R.; Cloran, F.; Bondo, F.; Bondo, G.; Hertz, B.; Carmichael, I.; Serianni, A. J Am Chem Soc 1998, 120, 11158–11173.

11. Cloran, F.; Carmichael, I.; Serianni, A. S. J Am Chem Soc. 1999, 121, 9843–9851.
12. Cloran, F.; Carmichael, I.; Serianni, A. S. J Phys Chem 1999, 103, 3783–3795.
13. Lipari, G.; Szabo, A. J Am Chem Soc 1982, 104, 4546–4559.
14. Lipari, G.; Szabo, A. J Am Chem Soc 1982, 104, 4559–4570.
15. Clore, G. M.; Szabo, A.; Bax, A.; Kay, L. E.; Driscoll, P. C.; Gronenborn, A. M. J Am Chem Soc 1990, 112, 4989–4991.
16. Tylianakis, M.; Spyros, A.; Dais, P.; Taravel, F. R.; Perico, A. Carbohydr Res 1999, 315, 16–34.
17. Perico, A.; Mormino, M.; Urbani, R.; Cesaro, A.; Tylianakis, E.; Dais, P.; Brant, D. A. J Phys Chem B 1999, 103, 8162–8171.
18. Xu, Q.; Bush, C. A. Biochemistry, 1996, 35, 14512–14520.
19. Gitti, R.; Long, G. X.; Bush, C. A. Biopolymers, 1994, 34, 1327–1338.
20. Cisar, J. O.; Sandberg, A. L.; Abeygunawardana, C.; Reddy, G. P.; Bush, C. A. Glycobiology 1995, 5, 655–662.
21. Abeygunawardana, C.; Bush, C. A.; Cisar, J. O. Biochemistry, 1990, 29, 234–248.
22. Xu, Q.; Mohan, S.; Bush, C. A. Biopolymers, 1996, 38, 339–353.
23. Fesik, S. W.; Zuiderberg, E. R. P. J Magn Reson 1988, 78, 588–593.
24. Uhrin, D.; Brisson, J. R.; Maclean, L. L.; Richards, J. C.; Perry, M. B. J Biomol NMR 1994, 4, 615–630.
25. Bax, A.; Davis, D. G. J Magn Reson 1985, 65, 355–360.
26. Xu, Q.; Bush, C. A. Carbohydr Res 1998, 306, 335–339.
27. Bax, A.; Max, D.; Zax, D. J Am Chem Soc 1992, 114, 6923–6925.
28. Kay, L. E.; Nicholson, L. K.; Delaglio, F.; Bax, A.; Torchia, D. A. J Magn Reson 1992, 97, 359–375.
29. Yamazaki, T.; Muhandiram, R.; Kay, L. E. J Am Chem Soc 1994, 116, 8266–8278.
30. Lommerse, J. P. M.; Kroon-Batenburg, L. M. J.; Kamerling, J. P.; Vliegenthart, J. F. G. J Biomol NMR 1995, 5, 79–94.
31. Farrow, N. A.; Zhang, O.; Szabo, A.; Torchia, D. A.; Kay, L. E. J Biomol NMR 1995, 6, 153–162.
32. Ishima, R.; Nagyama, K. J Magn Reson. 1995, B108, 73–76.
33. Lefevre, J. F.; Dayie, K. T.; Peng, J. W.; Wagner, G. Biochemistry 1996, 35, 2674–2686.
34. Jin, D.; Figueirido, F.; Montelione, G. T.; Levy, R. M. J Am Chem Soc 1997, 119, 6923–6924.
35. Xu, Q.; Bush, C. A. Biochemistry 1996, 35, 14521–14529.
36. Hajduk, P. J.; Horita, D. A.; Lerner, L. E. J Am Chem Soc 1993, 115, 9196–9201.
37. Ott, K. H.; Meyer, B. Carbohydr Res 1996, 281, 11–34.
38. Poveda, A.; Asensio, J. L.; Martin-Pastor, M.; Jimenez-Barbero, J. J Biomol NMR 1997, 10, 29–43.
39. Liu, Q.; Schmidt, R. K.; Teo, B.; Karplus, P. A.; Brady, J. W. J Am Chem Soc 1997, 119, 7851–7862.
40. Brant D. A.; Liu, H. S.; Zhu, Z. S. Carbohydr Res 1995, 278, 11–26.
41. Maler, L.; Widmalm, G.; Kowalewski, J. J Biomol. NMR, 1996, 7, 1–7.
42. Kjelberg, A.; Rundlof, T.; Kowalewski, J.; Widmalm, G. J Phys Chem B 1998, 102, 1013–1020.
43. Wu, J.; Bondo, P. B.; Vuorinen, T.; Serianni, A. S. J Am Chem Soc 1992, 114, 3499–3505.